The 2009 IEEE/RSJ International Conference on
Intelligent Robots and Systems
October 11-15, 2009 St. Louis, USA

Design and Characterization of a 7-DOF Haptic Interface for a Minimally Invasive Surgery Test-bed

H. Bassan[1,3], A. Talasaz[1,3] and R.V. Patel[1,2,3]
[1]Department of Electrical & Computer Engineering, [2]Department of Surgery, The University of Western Ontario,
and
[3]Canadian Surgical Technologies & Advanced Robotics (CSTAR),
London, Ontario, Canada.
{hbassan, atalasaz, rvpatel}@uwo.ca

Abstract— **In this paper, we present the design of a 7 degrees-of-freedom (DOF) Haptic Interface for applications in Minimally Invasive Surgery (MIS). The design of the interface is based on an existing dual-panthograph Haptic Wand and is capable of position and force reflection in three translational, three rotational DOF and grasping motion. The paper presents the implementation of a novel cable driven differential transmission to include the yaw and grasping force reflection to the interface. The kinematic and dynamic properties of the interface are characterized and presented. Experimental results demonstrate that the device is capable of high-force reflection with good transparency.**

Keywords: Haptic interface, force-feedback, minimally invasive surgery.

I. Introduction

MIS is gaining interest currently due to its benefits to the patient and the healthcare system. As opposed to open surgery, this approach utilizes thin instruments and an endoscope to perform surgery through tiny incisions on the patient's body. The approach is beneficial in terms of reduced trauma and scarring, faster recovery times and shorter hospital stays. In recent years, master-slave (tele-operated) robotic systems have been introduced to assist a surgeon perform MIS procedures. While the currently used robotic MIS systems (such as the da Vinci from Intuitive Surgical) do not have haptic feedback, in general, the master manipulator (haptic interface) of an MIS robotic system would be required to have force-reflection capability in all seven DOF (three translations, three rotations and grasping).

Various researchers have investigated experimental robotic test-beds for MIS. These systems utilize specialized surgical instruments (equipped with a force sensing capability) to provide force feedback to the operator using a haptic interface. In [1], a 7-DOF haptic interface for applications in robot-assisted MIS is presented. The device is capable of force reflection in 4-DOF and position sensing in 7-DOF. A haptic interface capable of force reflection in 5-DOF for MIS is presented in [2]. The design utilizes an off-the-shelf 3-DOF commercial haptic interface [3] and a custom designed grasping and roll assembly. In [4], a 7-DOF haptic interface based on a parallel kinematic structure is presented. The device has a large number of links arranged as a dual 3-legged structure and is capable of force feedback in 7-DOF.

A few commercial haptic interfaces with 7-DOF are available in the market. The Freedom 7S (MPB Technologies, Montreal, Canada) is a haptic interface with a 7-DOF force reflection capability. The device is available with a scissor like end-effector or an optional handle or a scalpel. However, this device is capable of very limited continuous force reflection due to the direct-drive actuators employed in the design. Another commercial haptic device with 6-DOF force reflection and 7-DOF position sensing is the PHANToM (Sensable Technologies, MA, U.S.A.). The grasping motion in this device is passive and is available either as a thumb-pad or a scissor like handle. Based on a parallel kinematic structure for positioning and a serial-chain structure for orientation, Omega (Force Dimension, Nyon, Switzerland) is another commercial haptic interface capable of force reflection in 7-DOF.

These haptic devices have limited applicability in MIS research due to one or more of the following shortcomings: insufficient DOF, limited continuous force reflection, limited workspace or high cost. Our research group (in collaboration with an industrial partner) has embarked on the development of an experimental test-bed for MIS where tool-tissue interaction is reflected to the surgeon through a custom designed haptic interface. In addition to robot-assisted master-slave MIS systems, the proposed haptic device is also suitable for application in surgical simulators (tip control similar to the da Vinci interface). In that scenario, the trainee clinician interacts with a virtual anatomy on a computer using virtual surgical tools to gain experience with the procedure. The proposed device will also be of particular interest to other researchers in the field of robotics, tele-operation and MIS as it provides a platform with seven DOF force reflection with a fairly simplistic mechanism and relatively low cost of construction as compared to existing devices. The tradeoff is a slightly lower range of motion in two orientation DOF.

II. Design and Development

The kinematic design of the proposed haptic interface is based on a dual-pantograph mechanism [5] (commercially

This research was supported by the Ontario Centers of Excellence under grant IC50272, and the Natural Sciences and Engineering Research Council (NSERC) of Canada under Grant CRDPJ349675-06.

available as the Haptic Wand [6] from Quanser Consulting Inc., Markham, Canada). The device is available with 5-DOF position and force-feedback capability and employs direct-drive actuators to minimize friction and maximize transparency. The haptic interface is controlled by linear current amplifiers to minimize actuator heating and therefore can provide higher force reflection for prolonged periods while minimizing electrical interference. The kinematic structure of the original Haptic Wand utilizes dual-panthograph mechanisms interfaced to the output handle through two Carden joints. Each closed-chain panthograph mechanism is actuated through the use of two shoulder motors which are supported on a single DOF waist joint resulting in a kinematic chain with three DOF. The addition of a Carden joint at each end of the handle constrains the total DOF of the haptic interface to five (three translation and two rotation: roll and pitch) with a redundant waist joint that eliminates a workspace singularity of the mechanism. The motion about the handle axis in the original device is passive and un-encoded. The pantograph linkages are built of a carbon-fiber material to minimize inertia, and two counterbalance weights are utilized to gravity balance individual pantograph mechanism in the middle of the workspace. The remaining gravity compensation torque (throughout the workspace) is provided using the actuators.

A. Hardware Modifications

The original haptic wand was found to have limited applicability in MIS due to the lack of force reflection in the yaw direction and grasping. Thus, it was required to modify the device to include force reflection in those DOF. Various design modifications were explored and their effects on the device performance were examined. A common approach would have been to redesign the output handle to include two actuators that would provide decoupled force reflection in the yaw and grasping. This approach however, would result in increased handle mass and therefore higher inertia and reduced force reflection capability and transparency. Even though it was possible to compensate for the increased mass to a certain extent by incorporating extra counterbalance weights, the particular kinematics of the haptic wand made it difficult to fully eliminate the effect. Increased handle mass would also have made it difficult for the user to manipulate the device for prolonged periods, a common requirement in surgical scenarios.

A novel and more elegant approach was devised to include the required DOF to the haptic wand. In this approach, the output handle of the haptic interface was designed to have two split sections, each attached to a corresponding pinch lever (end effector). Two handle drive actuators (Maxon motors RE35, 1.07Nm stall torque) were included in the mechanism, each independently controlling the corresponding handle. The resulting design is symmetrical about a horizontal plane and required minimal modifications to the existing components of the haptic wand. Figure 1 shows the CAD rendering of the modified 7-DOF haptic wand.

Figure 2 shows the close-up view of one pantograph mechanism with its associated handle drive transmission. A

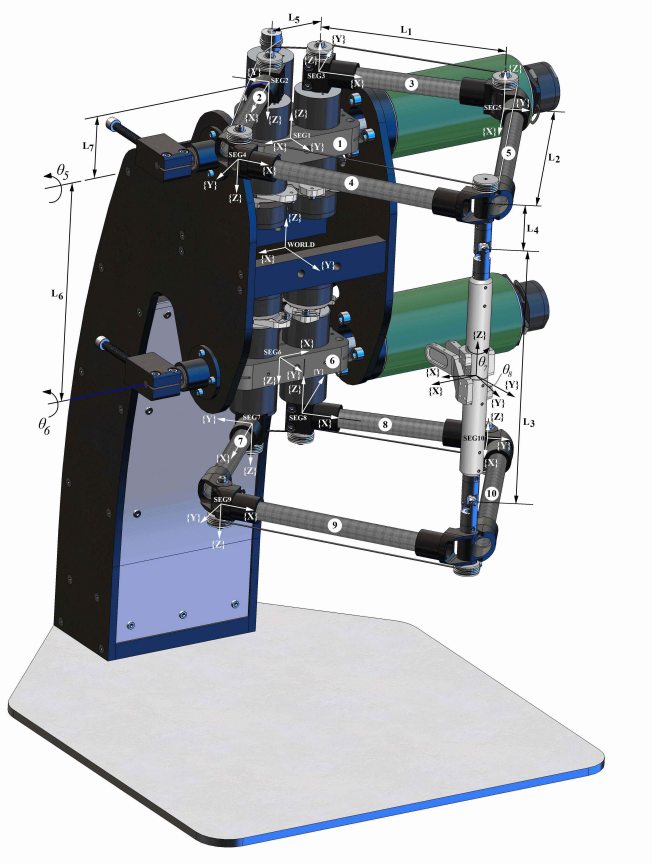

Fig. 1. CAD rendering of the modified 7-DOF Haptic Wand.

cable transmission (Gorilla^{TM} Tough fishing line, Berkley fishing, 50lb breaking strength) was utilized to transfer motor torques to the drive pulley in this design. This approach had the benefit that it allowed the handle drive motor to be located on the other side of the waist axis and therefore act as a counterweight to the pantograph linkages. The introduction of the handle drive motors as counterweights eliminated the need of the original counterweights, which were therefore removed from the device. Four idler pulleys were introduced in each pantograph at the shoulder and elbow joints to assist with cable routing. The cable windup drum on the handle drive motor was designed as having two split sections which facilitated in proper tensioning of the cable. One end of the cable loop was terminated on the first windup drum section, wrapped over shoulder and elbow idler pulleys a few turns and then terminated at the drive pulley. Similarly, the other end of the cable loop was terminated on the second windup drum section, wrapped over the other shoulder and elbow idler pulleys a few turns and then terminated at the drive pulley to complete the loop. The actuator torque was therefore transferred from the handle drive motor utilizing the cable transmission to the drive pulley in a continuous fashion.

Figure 3 shows the sectional view of the Carden joint drive of each pantograph. The drive shaft is supported by four idler bearings to create a passive joint with the pantograph

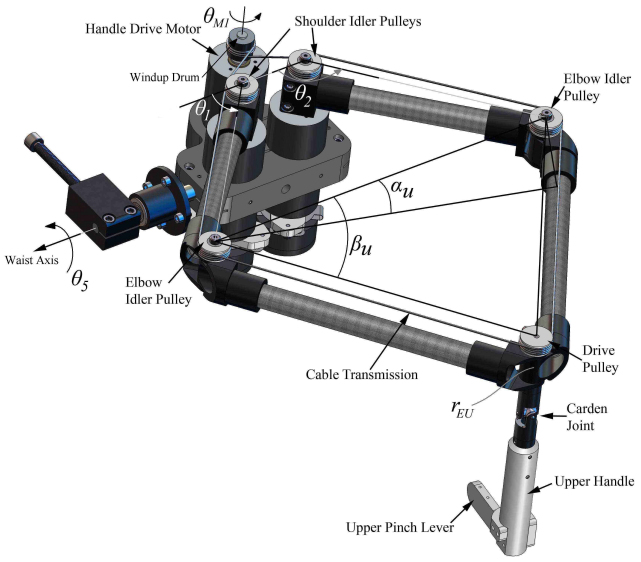

Fig. 2. CAD rendering of the upper handle drive.

mechanism and therefore can be independently rotated with respect to the pantograph. At each end, the drive shaft is firmly attached to the drive pulley and the input link of the Carden joint, respectively. The output link of the Carden joint is firmly attached to the handle and therefore actuator torque is transferred from the drive pulley through the drive shaft, through the carden joint to the handle and to the corresponding pinch lever.

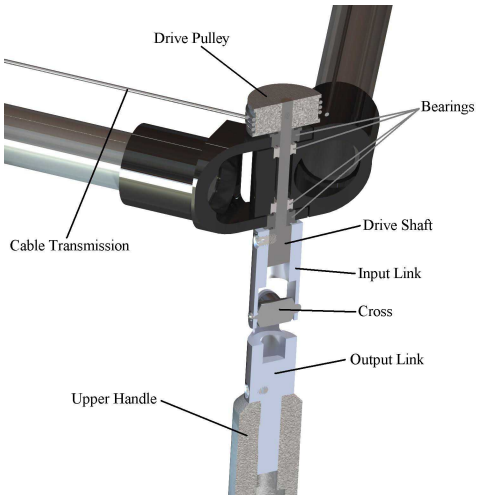

Fig. 3. Section view of the carden joint drive.

The upper and lower handles are coupled to each other through a passive joint (with its axis aligned with the longitudinal axes of the handles). In a typical setting, the user would hold the pinch levers utilizing the thumb and the index finger and could utilize the remaining fingers and palm to hold onto one of the handles for a better support. Velcro straps are attached to the pinch levers to maintain a firm contact with user's fingers at all times. The pinch levers were designed to be removable and can be easily replaced with other types of end-effectors (such as scissor handles etc), if required. The handles, pinch levers and idler pulleys were all manufactured using a rapid prototyping 3D printer (light weight ABS plastic material). Figure 4 shows the 7-DOF haptic wand.

The upper and lower pinch levers are individually actuated by the corresponding motors, however, as the user grasps the levers using the thumb and the index finger, a differential mechanism is created between the two. The yaw angle in the tool frame, denoted as θ_7 (Figure 1), is defined in the right-handed sense about the haptic wand handle and the grasp angle, denoted as θ_8, is the angle between the upper and lower pinch levers. The motion in the yaw and the grasping directions can be measured as follows:

$$\theta_7 = \frac{\theta_{M1} - \theta_{M2}}{2} \tag{1}$$

and

$$\theta_8 = -(\theta_{M1} + \theta_{M2}) \tag{2}$$

where θ_{M1} (Figure 2) and θ_{M2} are the right-handed angle of the upper and lower pinch lever actuators, respectively. The output torque in the yaw and grasping directions in terms of upper and lower actuator torques are then given by:

$$\tau_7 = \frac{\tau_{M1} - \tau_{M2}}{2} \tag{3}$$

and

$$\tau_8 = \frac{\tau_{M1} + \tau_{M2}}{2} \tag{4}$$

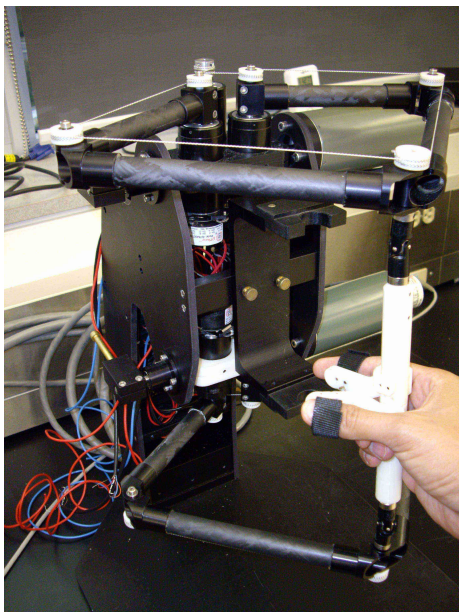

Fig. 4. 7-DOF Haptic Wand.

B. Forward Kinematics

The forward kinematics of the manipulator describe the end effector position and orientation with reference to a world frame as a function of its joint angles. For ease of kinematic and dynamic analyses, Figure 1 indicates the world

frame and segments 1 through 11 with their respective local coordinate systems (SEG_{1-11}). These segments include the top triple motor assembly, top left drive arm, top right drive arm, top left passive arm, top right passive arm, bottom triple motor assembly, bottom left drive arm, bottom right drive arm, bottom left passive arm and bottom right passive arm, labelled as 1 through 11, respectively. The haptic wand end effector is located in the middle of the handle and the tool coordinate system is parallel to the global coordinate system at the home position. The parameters $L_1, \ldots, L_7$ are defined as the distance between various frames. To solve the forward kinematics of the haptic wand, the problem is broken down into two smaller problems, i.e., forward kinematics for the upper pantograph and the lower pantograph, with end points (r_{EU} and r_{EL}) defined for these subsystems (see Figure 2).

Now referring to Figure 1, for the upper pantograph:

$$r_{SEG1} = \begin{bmatrix} 0 \\ 0 \\ \frac{L_6}{2} \end{bmatrix} \tag{5}$$

$$r_{SEG2} = \begin{bmatrix} \frac{L_5}{2} \\ -s_5 L_7 \\ \frac{L_6}{2} + c_5 L_7 \end{bmatrix} \tag{6}$$

$$r_{SEG3} = \begin{bmatrix} -\frac{L_5}{2} \\ -s_5 L_7 \\ \frac{L_6}{2} + c_5 L_7 \end{bmatrix} \tag{7}$$

$$r_{SEG4} = \begin{bmatrix} \frac{L_5}{2} + c_1 L_1 \\ -s_5 L_7 + c_5 s_1 L_1 \\ \frac{L_6}{2} + c_5 L_7 + s_5 s_1 L_1 \end{bmatrix} \tag{8}$$

$$r_{SEG5} = \begin{bmatrix} -\frac{L_5}{2} + c_2 L_1 \\ -s_5 L_7 + c_5 s_2 L_1 \\ \frac{L_6}{2} + c_5 L_7 + s_5 s_2 L_1 \end{bmatrix} \tag{9}$$

where, for $i = 1, .., 5$, r_{SEGi} is the origin of the frame attached to the SEG_i with respect to the world coordinate system and c_i and s_i stand for $\cos(\theta_i)$ and $\sin(\theta_i)$, respectively.

Referring to Figure 2, the position of the upper end point is computed as:

$$\alpha_U = \arctan \frac{s_1 L_1 - s_2 L_1}{L_5 + c_1 L_1 - c_2 L_1} \tag{10}$$

and

$$\beta_U = \arccos \frac{h_U}{2L_2} \tag{11}$$

where

$$h_U = \|r_{SEG4} - r_{SEG5}\| \tag{12}$$

Now, define

$$\psi_U = \pi - (\beta_U - \alpha_U) \tag{13}$$

and

$$\gamma_U = \alpha_U + \beta_U \tag{14}$$

then, we get

$$r_{EU} = r_{SEG4} + R_x(\theta_5) R_z(\psi_U) \begin{bmatrix} L_2 \\ 0 \\ -L_4 \end{bmatrix} \tag{15}$$

where, $R_j(\kappa)$ represents a rotation matrix about an axis j through an angle κ. Similarly, for the lower end point we get

$$r_{EL} = r_{SEG9} + R_x(\theta_6) R_z(\psi_L) \begin{bmatrix} L_2 \\ 0 \\ L_4 \end{bmatrix} \tag{16}$$

The haptic wand end effector is located in the middle of a straight line between the upper and lower end points (r_{EU} and r_{EL}). Therefore, we have

$$r_{EE} = r_{EL} + \frac{r_{EU} - r_{EL}}{2} \tag{17}$$

where r_{EE} is the position of the haptic wand end effector.

To calculate the orientation of the end effector, the roll, pitch and yaw angles are defined in the right-hand sense about the world X, Y and Z axes, respectively. Let us define a unit vector of the handle in the global frame as

$$u_h = \frac{r_{EU} - r_{EL}}{\|r_{EU} - r_{EL}\|} \tag{18}$$

and

$$G = R_z(-\psi_L) R_x(-\theta_6) \begin{bmatrix} 0 & 0 & u_h \end{bmatrix} R_z(-\theta_7) \tag{19}$$

by defining

$$\mu = \arctan \frac{G(1,3)}{G(3,3)} \tag{20}$$

and

$$\upsilon = -\arcsin G(2,3) \tag{21}$$

we can then compute

$$R_{EE} = R_x(\theta_6) R_z(\psi_L) R_y(\mu) R_x(\upsilon) R_z(\theta_7) \tag{22}$$

from 22, we can derive the Euler angles (about the world frame axes) using the following

$$o_{roll} = \arctan \frac{R_{EE}(3,2)}{R_{EE}(3,3)} \tag{23}$$

$$o_{pitch} = \arctan \frac{-R_{EE}(3,1)}{\sqrt{1 + R_{EE}(3,1)}} \tag{24}$$

$$o_{yaw} = \arctan \frac{R_{EE}(2,1)}{R_{EE}(1,1)} \tag{25}$$

C. Dynamics

The dynamic equations of the haptic wand are derived using the Lagrangian formulation. The location of the center of mass for segment $\{i\}$ in the local frame, r^l_{cmi}, can be expressed in world coordinates, r^w_{cmi}, as

$$r^w_{cmi} = r^w_{oi} + R_x(\phi_i)\, R_z(\varphi_i)\, r^l_{cmi} \tag{26}$$

where r^w_{oi} is the position of the origin of the local frame for segment $\{i\}$ and ϕ_i is equal to θ_5 for the upper pantograph,

θ_6 for the lower pantograph and 0 for the handle. we also have

$$\varphi = \begin{bmatrix} 0 & \theta_1 & \theta_2 & \psi_U & \gamma_U & 0 & \theta_3 & \theta_4 & \psi_L & \gamma_L & \chi \end{bmatrix}$$

Since the origin of the tool frame is coincident with the center of mass of the handle, we have $r^l_{cm11} = 0$. For $i = 1, 6$, $r^l_{cmi} = \begin{bmatrix} 0 & -l_{cmi} & 0 \end{bmatrix}^T$ and for the other segments $r^l_{cmi} = \begin{bmatrix} l_{cmi} & 0 & 0 \end{bmatrix}^T$.

The rotational velocity, Ω_i for $i = 1, \ldots, 11$, in local frames is given by

$$\Omega_1 = \begin{bmatrix} \omega_5 \\ 0 \\ 0 \end{bmatrix} \qquad \Omega_6 = \begin{bmatrix} \omega_6 \\ 0 \\ 0 \end{bmatrix} \qquad \Omega_{11} = \begin{bmatrix} 0 \\ 0 \\ \omega_{11} \end{bmatrix} \tag{27}$$

$$\Omega_2 = \begin{bmatrix} c_1\omega_5 \\ -s_1\omega_5 \\ \omega_1 \end{bmatrix} \qquad \Omega_3 = \begin{bmatrix} c_2\omega_5 \\ -s_2\omega_5 \\ \omega_2 \end{bmatrix} \tag{28}$$

$$\Omega_7 = \begin{bmatrix} c_3\omega_6 \\ -s_3\omega_6 \\ \omega_3 \end{bmatrix} \qquad \Omega_8 = \begin{bmatrix} c_4\omega_6 \\ -s_4\omega_6 \\ \omega_4 \end{bmatrix} \tag{29}$$

$$\Omega_4 = R_z(-\psi_U)\,\Omega_1 + \begin{bmatrix} 0 \\ 0 \\ \dot{\psi_U} \end{bmatrix} \tag{30}$$

$$\Omega_5 = R_z(-\gamma_U)\,\Omega_1 + \begin{bmatrix} 0 \\ 0 \\ \dot{\gamma_U} \end{bmatrix} \tag{31}$$

$$\Omega_9 = R_z(-\psi_L)\,\Omega_6 + \begin{bmatrix} 0 \\ 0 \\ \dot{\psi_L} \end{bmatrix} \tag{32}$$

$$\Omega_{10} = R_z(-\gamma_L)\,\Omega_6 + \begin{bmatrix} 0 \\ 0 \\ \dot{\gamma_L} \end{bmatrix} \tag{33}$$

The translational velocity is also defined for the center of mass vector and is calculated as

$$v_{cmi} = \dot{r}_{cmi} \quad \text{for} \quad i = 1, \cdots, 11$$

The kinetic energy for each segment is given by

$$K_i = \frac{1}{2}(v^T_{cmi}\, M_i\, v_{cmi} + \Omega^T_i\, I_i\, \Omega_i) \tag{34}$$

where $M_i = m_i\, I_{3\times 3}$ and I_i are respectively the translational and rotational inertia matrices for $i = 1, .., 11$. The potential energy for the segment $\{i\}$ is defined as

$$V_i = m_i\, g\, r^z_{cmi} \tag{35}$$

where r^z_{cmi} is the third element of the vector r_{cmi} (Z direction). Then the lagrangian for the haptic wand is given by

$$L = \sum_{i=1}^{11} K_i - \sum_{i=1}^{11} V_i \tag{36}$$

and, the dynamic equations are calculated from

$$\frac{d}{dt}\frac{\partial L}{\partial \dot{\theta_i}} - \frac{\partial L}{\partial \theta_i} = \tau_i, \quad i = 1, .., 7. \tag{37}$$

TABLE I

HAPTIC WAND PARAMETERS

i	$m_i(kg)$	$l_{cmi}(m)$	$L_i(m)$
1	1.1000	0.011	0.1443
2	0.0601	0.042	0.1961
3	0.0601	0.042	0.2114
4	0.0543	0.090	0.0359
5	0.0581	0.090	0.0445
6	1.1000	0.011	0.1778
7	0.0601	0.042	0.0526
8	0.0601	0.042	–
9	0.0543	0.090	–
10	0.0581	0.090	–
11	0.0637	–	–

TABLE II

HAPTIC WAND WORKSPACE

Translation (mm)	480W x 450H x 250D
Rotation (deg)	±85 (roll) ±65 (pitch) ±160 (yaw) 30 (grasp)

D. Haptic Wand Parameters

The pantograph links of the haptic interface are made up of hollow carbon fiber tubing and therefore have negligible mass and inertia. For simplicity of the dynamic model, these parameters are excluded from the calculations and only the inertia of the motor assemblies in the following form, expressed in local frames, are utilized.

$$\begin{bmatrix} I_{ixx} & 0 & 0 \\ 0 & I_{iyy} & 0 \\ 0 & 0 & I_{izz} \end{bmatrix} \qquad i = 1, 6. \tag{38}$$

At the same time, the rotational velocity for the upper and lower motor assemblies is only about the X-axis and as a result, only $I_{1xx},\ I_{6xx}$ are involved in the kinetic energy calculation. The measured values for these parameters (in $kg\ m^2$) are

$$I_{1xx} = 0.00163 \qquad I_{6xx} = 0.00163$$

The other parameters for the 7-DOF haptic wand are summarized in Table I and the workspace is given in Table II.

III. EXPERIMENTS

To evaluate the closed-loop performance and measure the transparency of force reflection, the kinematic and dynamic models developed in sections II-B and II-C were utilized to create a virtual wall simulation for the haptic interface [7]. An impedance control algorithm as shown in Figure 5 was implemented for the experiments reported in this paper.

The impedance controller was designed so as to match the dynamics of the haptic wand with those of the virtual wall. The wall was assumed to be linear and decoupled in each coordinate and therefore, a simplified decoupled controller was designed for each DOF. The decoupled controllers require velocity feedback in world coordinates (linear and angular) that was derived from the joint velocities of the motors and the Jacobian of the haptic wand. The joint velocities were

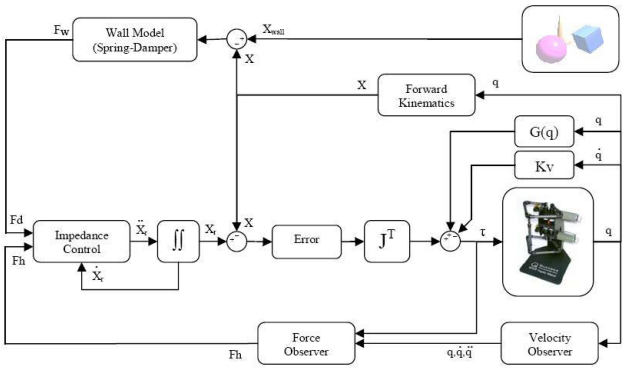

Fig. 5. Control block diagram for 7-DOF haptic wand including virtual environment.

estimated from the encoder measurements using a velocity observer. The interaction force between the haptic wand and the operator's hand was measured by a force observer that was designed based on the obtained dynamics of the haptic wand [8]. In order to precisely transfer the simulated forces from the virtual wall to the operator, the gravity terms were extracted from the dynamics equations and fed forward to the controller.

The virtual wall [9] was modeled as a spring-damper system and using this model, the reaction wall force can be computed as

$$F_w = -\zeta[K_w(X - X_w) + \gamma B_w \dot{X}] \tag{39}$$

where K_w and B_w are the spring and damper constants, respectively and ζ and γ are defined as

$$\zeta = \begin{cases} 1 & X > X_w \\ 0 & X \leq X_w \end{cases} \quad \gamma = \begin{cases} 1 & \dot{X} > 0 \\ 0 & \dot{X} \leq 0 \end{cases} \tag{40}$$

The parameter ζ guarantees that no force is exerted on the end effector unless the handle penetrates the virtual wall. Simultaneously, selecting γ as given in (40) ensures that no extra force is applied to the operator's hand when the handle is being removed from the wall.

Figures 6 and 7 show the tracking response of the haptic interface for three translational and three rotational DOF, respectively. The handle was kept in a fixed position during the experiment. In order to evaluate the transparency of force reflection, the following values for environment stiffness were selected:

$$K_w = \begin{cases} 500 & t \leq 30 \\ 1000 & t > 50 \end{cases} \tag{41}$$

It can be seen from Figures 6 and 7 that the interaction force between the haptic wand and the operator's hand correspond accurately to the force reflected from the virtual wall.

IV. Conclusion

In this paper, we have presented the design, development and modeling of a seven-DOF haptic interface for minimally invasive surgery. An existing 5-DOF haptic interface was

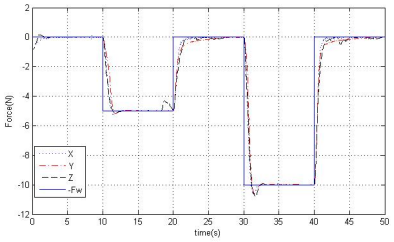

Fig. 6. Tracking response for translational DOF.

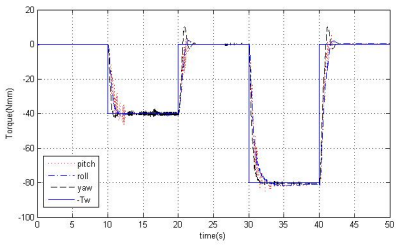

Fig. 7. Tracking response for rotational DOF.

modified to include force-feedback in the yaw and grasping directions through the use of a highly-backdrivable cable-driven differential transmission. The kinematic and dynamic analyses of the modified interface was presented. Future work will involve integration of the haptic interface into a master-slave robotic test-bed to evaluate haptic-based tele-manipulation.

V. Acknowledgements

The authors would like to thank Jacob Apkarian, Ryan Leslie and Paul Karam at Quanser Consulting Inc., for help with the QuaRC software and the kinematics and dynamics of the 5-DOF Haptic Wand.

References

[1] G. Tholey and J. P. Desai, "A general-purpose 7 DOF haptic devive: Applications toward robot-assisted surgery," *IEEE/ASME Transactions on Mechatronics*, vol. 12, pp. 662–669, Dec. 2007.

[2] M. Tavakoli, R. Patel, M. Moallem, and A. Aziminejad, *Haptics-Based Systems for Robot-Assisted Surgery and Telesurgery: Design, Control, and Experimentation*. World Scientific Publishers in the series - New Frontiers in Robotics, 2008.

[3] T. H. Massie and J. K. Salisbury, "Force reflecting haptic interface," in *U.S. patent 5,625,576*, 1999.

[4] K. Kim, W. K. Chung, and Y. Youm, "Design and analysis of a new 7-DOF parallel type haptic device : PATHOS-II," in *IEEE/RSJ Conference on Intelligent Robots and Systems*, pp. 2241–2246, 2003.

[5] L. J. Stocco, S. E. Salcudean, and F. Sassani, "Optimal kinematic design of a haptic pen," *IEEE/ASME Transactions on Mechatronics*, vol. 6, pp. 210–220, Sept. 2001.

[6] http://www.quanser.com.

[7] M. R. Sirouspour, S. P. DiMaio, S. E. Salcudean, P. Abolmaesumi, and C. Jones, "Haptic interface control-design issues and experiments with a planar device," in *IEEE International Conference on Robotics and Automation*, pp. 789–794, 2000.

[8] A. C. Smith, F. Mobasser, and K. Hashtrudi-Zaad, "Neural-network-based contact force observers for haptic applications," *IEEE Transactions on Robotics*, vol. 22, pp. 1163–1175, Dec. 2006.

[9] J. Yoon and J. Ryu, "Control and evaluation of a new 6-dof haptic device using a parallel mechanism," in *IEEE/RSJ Conference on Intelligent Robots and Systems*, pp. 1125–1130, 2000.